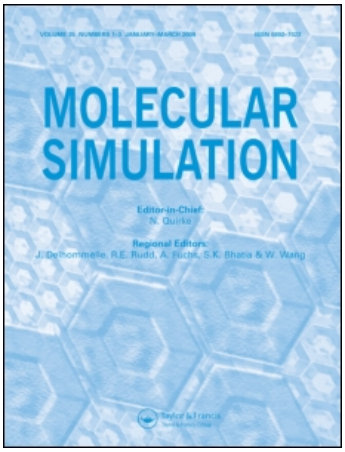

Molecular Simulation
Publication details, including instructions for authors and subscription information:
http://www.informaworld.com/smpp/title~content=t713644482

Accurate Kirkwood-Buff integrals from molecular simulations

Rasmus Wedberg[a]; John P. O'Connell[b]; Günther H. Peters[c]; Jens Abildskov[a]
[a] Department of Chemical and Biochemical Engineering, Technical University of Denmark, Lyngby, Denmark [b] Department of Chemical Engineering, University of Virginia, Charlottesville, VA, USA [c] Department of Physics, MEMPHYS - Centre for Biomembrane, Odense, Denmark

First published on: 02 November 2010

To cite this Article Wedberg, Rasmus , O'Connell, John P. , Peters, Günther H. and Abildskov, Jens(2010) 'Accurate Kirkwood-Buff integrals from molecular simulations', Molecular Simulation, 36: 15, 1243 — 1252, First published on: 02 November 2010 (iFirst)
To link to this Article: DOI: 10.1080/08927020903536366
URL: http://dx.doi.org/10.1080/08927020903536366

Molecular Simulation
Vol. 36, No. 15, December 2010, 1243–1252

Taylor & Francis
Taylor & Francis Group

Accurate Kirkwood–Buff integrals from molecular simulations

Rasmus Wedberg[a], John P. O'Connell[b], Günther H. Peters[c] and Jens Abildskov[a]*

[a]*Department of Chemical and Biochemical Engineering, Technical University of Denmark, Kgs. Lyngby, Denmark;* [b]*Department of Chemical Engineering, University of Virginia, Charlottesville, VA, USA;* [c]*Department of Physics, MEMPHYS – Centre for Biomembrane, Odense, Denmark*

(*Received 1 September 2009; final version received 7 December 2009*)

A method is proposed for obtaining thermodynamic properties via Kirkwood–Buff (KB) integrals from molecular simulations. In order to ensure that the KB integration converges, the pair distribution function is extrapolated to large distances using the extension method of Verlet, which enforces a theoretical limiting behaviour on the corresponding direct correlation function. The method is evaluated for the pure Lennard-Jones and Stockmayer fluids. The results are verified by comparing pure fluid isothermal compressibilities obtained from the KB integrals with values from derivatives of equations of state fitted to simulation results. Good agreement is achieved for both fluids at densities larger than 1.5 times the critical density.

Keywords: fluctuation solution theory; Kirkwood–Buff integrals; NVT simulations

1. Introduction

Molecular simulation is a powerful tool for predicting thermodynamic properties [1]. However, accurate calculation of useful properties, such as the excess Gibbs free energy, often requires the simulations to be carefully set up with extensive sampling [2]. A novel approach developed recently [3–5] allows thermodynamic properties of solutions to be evaluated using equations from fluctuation solution theory (FST) [6,7]. These equations relate such thermodynamic quantities to the Kirkwood–Buff (KB) integrals, i.e. spatial integrals of the pair correlation functions, which are directly obtained from molecular simulations. This approach allows for computing derivatives of several thermodynamic properties, namely isothermal compressibilities, partial molar volumes and derivatives of activities [7]. However, evaluating the KB integrals by direct numerical integration of the pair distribution functions is challenging. Firstly, the distribution functions are obtainable only over the system size, and it is unlikely that this range is sufficiently large to ensure convergence of the KB integrals. Secondly, the obtained distribution functions are likely to be inaccurate at large spatial separations due to finite-size effects, as discussed elsewhere [8]. Using a larger system might remedy this, but would significantly increase the computation time without necessarily ensuring accuracy. Several authors have pointed out these difficulties, and proposed ways of dealing with them. Weerasinghe and Smith [9] studied water–acetone mixtures by truncating the integrals outside a certain correlation region. Perera and Sokolić [10] and Hess and van der Vegt [11] both shifted the tail of the distribution function to ensure convergence of the integrals. In our recent studies [3–5,12], the tail of the distribution function was fitted to a parametric expression, determined by empirical means, which then was used to extend the simulation results to large spatial separations. Despite the successes of these efforts, we believe that a more robust procedure for extending the pair distribution function obtained from molecular simulations should be established from a theoretically well-justified approach with extensive quantitative testing.

The task of extending the pair distribution function based on theoretical considerations has been addressed in the literature [13–18], usually with the aim to study the correlation functions themselves or to calculate the structure factor. Verlet [13] developed a method in which the pair total correlation function (TCF) is extended by forcing the corresponding direct correlation function (DCF) at large separations to be consistent with a theoretical result. The approach used either the Mayer *f*-function or the Percus–Yevick (PY) relation to extend pair distribution functions obtained from simulations of the pure Lennard-Jones (LJ) fluid. Calculations of isothermal compressibilities by integration of the extended pair correlation functions were reported only for three state conditions, and Verlet [13] indicated that the statistical uncertainties were large. It is unclear whether these uncertainties were due to the quality of the simulations and their analysis or to the assumptions made by the extension method. Furthermore, while the obtained compressibilities were apparently compatible with the equation of state

*Corresponding author. Email: ja@kt.dtu.dk

ISSN 0892-7022 print/ISSN 1029-0435 online

DOI: 10.1080/08927020903536366
http://www.informaworld.com

(EOS) at the time, the thermodynamic property agreement was not reported in quantitative terms, as the focus of the paper was on other properties of the correlation functions.

In this work, we report a more thorough investigation of the accuracy of thermodynamic properties obtained from integrating correlation functions using Verlet's extension method [13]. In addition, we examine extension of the method to polar fluids, as the systems of ultimate interest in engineering applications, such as polar/non-polar mixtures, inevitably involve angle-dependent forces. To this end, we have analysed molecular dynamics (MD) simulations of the pure LJ and Stockmayer fluids for a wide range of state conditions, as studying model fluids allows straightforward assessment of the accuracy and limitations of the computed KB integrals.

2. FST in pure systems

Of central importance in FST are the TCF, $h(\mathbf{r}_{12}\omega_1\omega_2)$, and the DCF, $c(\mathbf{r}_{12}\omega_1\omega_2)$, where $\mathbf{r}_{12}$ denotes the spatial separation vector and ω_1 and ω_2 denote molecular orientations. The correlation functions can be related via the Ornstein–Zernike (OZ) equation [19]:

$$h(\mathbf{r}_{12}\omega_1\omega_2) = c(\mathbf{r}_{12}\omega_1\omega_2) + \rho\int\langle h(\mathbf{r}_{13}\omega_1\omega_3)c(\mathbf{r}_{32}\omega_3\omega_2)\rangle_{\omega_3}\,\mathrm{d}\mathbf{r}_3, \quad (1)$$

where $\langle\cdot\rangle_{\omega_3}$ denotes averaging over the orientation ω_3. Under certain conditions [19], the TCF and DCF for molecular centres, $h(r)$ and $c(r)$, defined by:

$$h(r) = \langle h(\mathbf{r}_{12}\omega_1\omega_2)\rangle_{\omega_1\omega_2} \quad (2)$$

and

$$c(r) = \langle c(\mathbf{r}_{12}\omega_1\omega_2)\rangle_{\omega_1\omega_2} \quad (3)$$

are related via the 'atomic' OZ equation which does not involve averaging over orientations,

$$h(r) = c(r) + \rho\int h(|\mathbf{r}-\mathbf{r}'|)c(r')\mathrm{d}\mathbf{r}'. \quad (4)$$

Equation (4) is fulfilled, e.g. for spherically symmetric potentials, but not rigorously for anisotropic potentials where $h(r)$ is coupled to the anisotropic part of $c(\mathbf{r}_{12}\omega_1\omega_2)$, and vice versa. Equation (4) seems to be a reasonable approximation, since decoupling occurs in, for example, the mean-spherical approximation treatment of the dipolar hard-sphere fluid, whose anisotropic part is identical to the Stockmayer fluid [19]. Also, success with modelling integrals of the DCF for complex substances suggests that this approximation can be satisfactory [20,21]. We explore this issue with the Stockmayer fluid, assuming that the coupling is negligible and that Equation (4) is a good approximation of the full OZ equation, Equation (1).

The TCF is related to the isothermal compressibility, κ_T, via the compressibility equation [22]:

$$\left(\frac{\partial\rho}{\partial p}\right)_T \equiv \rho\kappa_T = \frac{1}{k_BT}\left(1+4\pi\rho\int r^2h(r)\,\mathrm{d}r\right) \equiv \frac{1+H}{k_BT}, \quad (5)$$

where T and k_B denote temperature and the Boltzmann constant, respectively, and H defines the TCF integral (TCFI) or KB integral. When Equation (4) is valid, κ_T can also be expressed in terms of the DCF integral (DCFI) as

$$\left(\frac{\partial p}{\partial\rho}\right)_T \equiv \frac{1}{\rho\kappa_T} = k_BT\left(1-4\pi\rho\int r^2c(r)\,\mathrm{d}r\right) \equiv k_BT(1-C), \quad (6)$$

where C is the DCFI.

For multi-component solutions, h and c will be replaced by matrices of functions that represent correlations between the different components, and Equation (4) is replaced by a matrix equation [7]. The usefulness of FST is much greater for mixtures, where partial molar volumes and composition derivatives of activity coefficients are expressed in terms of the pair correlation function integrals [7]. This paper focuses only on pure fluids, so the simple notation in Equations (4)–(6) is retained.

3. Methods

3.1 Model fluids and MD simulations

We carry out simulations of two model fluids; one with intermolecular forces of the LJ form and the other with the Stockmayer potential. In the LJ fluid, the particles interact via a potential defined by [23]:

$$u_{LJ}(r_{ij}) = 4\epsilon\left[\left(\frac{\sigma}{r_{ij}}\right)^{12} - \left(\frac{\sigma}{r_{ij}}\right)^{6}\right], \quad (7)$$

where r_{ij} is the distance between particles i and j. In the Stockmayer fluid, each particle carries an electric dipole moment of magnitude μ. The interaction potential is given by [23]:

$$u_{SM}(\mathbf{r}_{ij},\hat{\mathbf{d}}_i,\hat{\mathbf{d}}_j) = u_{LJ}(\mathbf{r}_{ij}) + u_{dd}(\mathbf{r}_{ij},\hat{\mathbf{d}}_i,\hat{\mathbf{d}}_j), \quad (8)$$

where the second term is the dipole–dipole interaction that depends on the unit vectors $\hat{\mathbf{d}}_i$ and $\hat{\mathbf{d}}_j$, which give the directions of the dipole moments of the particles i and j, respectively, as well as the separation vector, $\mathbf{r}_{ij}$.

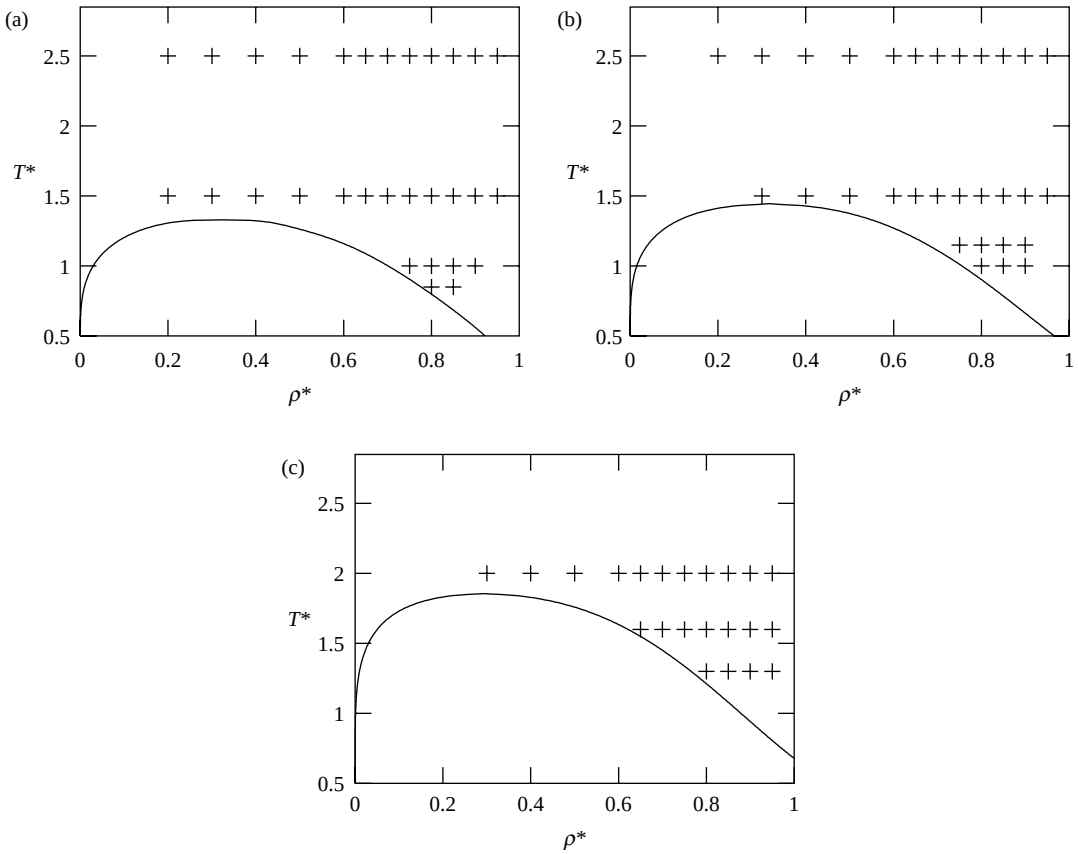

Figure 1. State points used in the simulations (+) using (a) the LJ fluid, (b) the Stockmayer fluid with $\mu^{*2} = 1$ and (c) the Stockmayer fluid with $\mu^{*2} = 3$. The boundary of the vapour–liquid coexistence region is indicated for each system and was obtained from the (a) Mecke and (b), (c) Gross EOS [28,29].

The interaction potential is defined by:

$$u_{\mathrm{dd}}(\mathbf{r}_{ij}, \hat{\mathbf{d}}_i, \hat{\mathbf{d}}_j) = \frac{\mu^2}{r_{ij}^3}\left[\left(\hat{\mathbf{d}}_i \cdot \hat{\mathbf{d}}_j\right) - 3\left(\hat{\mathbf{d}}_i \cdot \hat{\mathbf{r}}_{ij}\right)\left(\hat{\mathbf{d}}_j \cdot \hat{\mathbf{r}}_{ij}\right)\right]. \quad (9)$$

All simulations were carried out in the NVT ensemble using 864 molecules initially arranged according to an fcc lattice and with initial velocities assigned according to the Maxwell–Boltzmann distribution. The LJ parameters, σ and ϵ/k_{B}, were set to 3.405 Å and 119.8 K, respectively, and the molar mass, m, was set to 39.941 g/mol, which is the set of parameters commonly used to model argon. Periodic boundary conditions in all three dimensions were employed, and LJ forces were truncated at 4σ. In the LJ simulations, the velocity Verlet algorithm [24] with a time step of 2 fs was employed to integrate the equations of motion. The velocities were rescaled at each time step to maintain constant temperature. The systems were equilibrated for 100 ps and the production periods were 900 ps.

The simulations of the Stockmayer fluid were carried out using either $\mu^{*2} = 1$ or 3, where $\mu^{*2} = \mu^2 \epsilon^{-1} \sigma^{-3}$ denotes the reduced squared dipole moment. Electrostatic energies and forces were evaluated using the Ewald summation method with the parameter $\alpha = 3.5/L$, and the upper cut-off in reciprocal space, $n_{\mathrm{c}} = 6$, following the notation of Rapaport [25]. The fifth-order Nordsieck–Gear predictor–corrector method [24], with a time step of 2 fs, was employed to integrate the equations of motion. Rotational motion was implemented via the quaternion algorithm [24], where all particles were assigned a reduced moment of inertia of 0.1. The systems were equilibrated for 100 ps, and the production periods were 900 ps.

The state points simulated are summarised in Figure 1.

3.2 *Extending and integrating the TCF*

Verlet's method for extending the TCF [13] utilises the fact that c has a simpler structure and shorter range than h. Furthermore, for potentials that decay according to a power law faster than r^{-3}, the asymptotic behaviour of c is known to be [26]:

$$c(r) = -\beta u(r) + O((u(r))^2), \quad (10)$$

where u is the intermolecular potential and $\beta = (k_{\mathrm{B}}T)^{-1}$. In order to extend the TCF obtained from simulation, one

chooses a value R within the range for which $h(r)$ is sampled, and determines h and c such that:

$$\begin{cases} h(r) = h_{\mathrm{MD}}(r), & r \le R, \\ c(r) = a(u(r), h(r)), & r > R, \end{cases} \tag{11}$$

where h_{MD} denotes the TCF sampled in simulation and $a(u(r), h(r))$ is an explicit expression giving $c(r)$ in terms of $h(r)$ and $u(r)$. The requirements in Equation (11) together with the OZ equation, define a closed-form integral equation, which can be solved in order to obtain the $h(r)$, for $r > R$. Simultaneously, $c(r)$ is obtained for all r. In our implementation, h and c are discretised as linear splines and both functions are assumed to be zero for $r > 15\sigma$. The Fourier-transformed OZ equation [19] is employed to express c explicitly in terms of h. This transforms the integral equation into a system of non-linear equations for which a numerical solution is found using Newton's method [27]. The Jacobian is evaluated analytically; usually, 5–15 iterations are required for convergence. For the LJ fluid, three different relations $a(u(r), h(r))$ were investigated: the Mayer f-function [22],

$$a(u(r), h(r)) = f(r) \equiv \exp(-\beta u(r)) - 1, \tag{12}$$

the first-order virial expansion of c [22],

$$a(u(r), h(r)) = f(r)\left(1 + \rho \int f(|\mathbf{r} - \mathbf{r}'|) f(r')\, \mathrm{d}\mathbf{r}'\right), \tag{13}$$

and the PY relation [22],

$$a(u(r), h(r)) = (1 + h(r))(1 - \exp(\beta u(r))). \tag{14}$$

Note that all these theories for c are all consistent with the asymptotic result of Equation (10).

As will be discussed in Section 4.2, the three relations in Equations (12)–(14) yielded similar results for the isothermal compressibility for the LJ fluid. Therefore,with an accurate EOS, only the simplest relation, the Mayer f-function, was employed with the Stockmayer fluid. The f-function for a Stockmayer fluid depends on orientation as well as spatial separation. In order to obtain an approximation for the long-range behaviour of c that only depends on r, we integrate out the dependence on orientations, utilising that

$$\begin{aligned} \langle \exp(-\beta u_{\mathrm{dd}}(r, \hat{\mathbf{d}}_1, \hat{\mathbf{d}}_2)) \rangle_{\hat{\mathbf{d}}_1 \hat{\mathbf{d}}_2} &= 1 - \beta \langle u_{\mathrm{dd}}(r, \hat{\mathbf{d}}_1, \hat{\mathbf{d}}_2) \rangle_{\hat{\mathbf{d}}_1 \hat{\mathbf{d}}_2} \\ &\quad + \frac{\beta^2}{2} \langle u_{\mathrm{dd}}(r, \hat{\mathbf{d}}_1, \hat{\mathbf{d}}_2)^2 \rangle_{\hat{\mathbf{d}}_1 \hat{\mathbf{d}}_2} \\ &\quad - \frac{\beta^3}{6} \langle u_{\mathrm{dd}}(r, \hat{\mathbf{d}}_1, \hat{\mathbf{d}}_2)^3 \rangle_{\hat{\mathbf{d}}_1 \hat{\mathbf{d}}_2} \\ &\quad + O\left(\frac{\beta^4 \mu^8}{r^{12}}\right) \\ &= 1 + \frac{\beta^2 \mu^4}{3r^6} + O\left(\frac{\beta^4 \mu^8}{r^{12}}\right), \end{aligned}$$

since the first- and third-order terms in the Taylor expansion vanish when averaged over orientations. Truncating the expansion at second order, we obtain an approximate expression for the Mayer f-function averaged over orientations

$$\begin{aligned} \langle f(r, \hat{\mathbf{d}}_1, \hat{\mathbf{d}}_2) \rangle_{\hat{\mathbf{d}}_1 \hat{\mathbf{d}}_2} &= \exp(-\beta u_{\mathrm{LJ}}(r)) \\ &\quad \times \langle \exp(-\beta u_{\mathrm{dd}}(r, \hat{\mathbf{d}}_1, \hat{\mathbf{d}}_2)) \rangle_{\hat{\mathbf{d}}_1 \hat{\mathbf{d}}_2} - 1 \\ &\approx \exp(-\beta u_{\mathrm{LJ}}(r)) \left(1 + \frac{\beta^2 \mu^4}{3r^6}\right) - 1, \end{aligned}$$

which is employed as the approximation for the long-range behaviour of c.

3.3 EOS for verification of integrals

The computational method described in the previous section extends $h(r)$ and $c(r)$ to all values of r. These two functions can be integrated numerically to obtain the quantities H and C, and from either of these, the isothermal compressibility κ_{T} can be extracted using Equation (5) or (6). To assess the accuracy of κ_{T} computed in this way, we compare the result with accurate EOS obtained from correlating pressure, density and temperature of a large number of MD or Monte Carlo simulations. We use here the EOS by Mecke et al. [28] and Gross and Vrabec [29]. The isothermal compressibility is straightforwardly obtained by analytical differentiation of the EOS.

4. Results

Densities and temperatures given in this section are reduced with respect to σ, ϵ/k_{B} and m when marked with '$*$'. Overall, the simulations of the LJ fluid were found to be in very good agreement with the Mecke EOS [28]; deviations in pressure were $<1\%$ and typically around 0.2%. The Stockmayer simulations carried out with $\mu^{*2} = 1$ yielded pressures within 2% of those obtained from the Gross EOS [29]. For $\mu^{*2} = 3$, typical

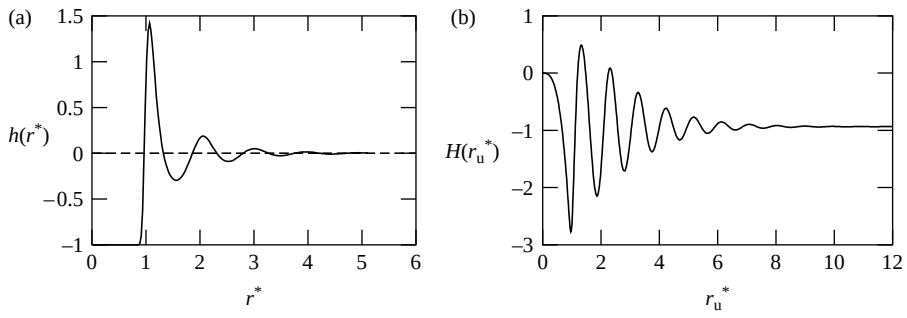

Figure 2. (a) TCF obtained from simulation of the LJ fluid at $T^* = 1.5$, $\rho^* = 0.8$ as a function of R^*. (b) The corresponding TCF integral as a function of upper integration limit, r_u^*. The TCF was extended according to Equation (11) prior to integration.

discrepancies in pressure were around 2–3%, although some were as large as 5–6% for a few state points at low reduced temperature.

4.1 Choosing R

We first note that direct numerical integration of the TCF did not converge for any of the systems we studied. Integration of the extended correlation function obtained from the method described in Section 3.2 did converge since it is carried out over a longer range of r, as shown in Figure 2(b). In contrast with Verlet's findings [13], the isothermal compressibilities obtained from our procedure depend on the value of R used in Equations (11). This is to be expected since if R is chosen too small, the asymptotic theory for c will be inaccurate, and if R is too large, h_{MD} will be used over a range where it is inaccurate. In order to establish a rational basis for selecting R, we consider the isothermal compressibility obtained from the KB integral as a function of $R^* \equiv R/\sigma$, $\alpha(R^*)$, using the simulation results for the LJ fluid. At all state points, and for each of the three relations for c (Equations (12)–(14)), it is found that $\alpha(R^*)$ has a clear negative slope on $R^* \in [1, 1.5]$, roughly between the location of the first peak and the second zero of h, as shown in Figure 2(a). Furthermore, the slope of $\alpha(R^*)$ is again negative on $R^* \in [3, 4]$, roughly after the fifth zero of h. In the region between, the behaviour of $\alpha(R^*)$ is different at different state points. When $\rho^* \geq 0.5$, a plateau-like region is found at about 1.8–2.2, as depicted in Figure 3, typically around the location of the third zero of h. While $\alpha(R^*)$ shows some variation on the plateau, the value stays within a few per cent of the plateau average. For $\rho^* \leq 0.4$, the plateau vanishes, and $\alpha(R^*)$ decreases monotonically as a function of R^*. We interpret the plateau seen in $\alpha(R^*)$ as an indication that R^* is small enough for $h_{MD}(r^*)$ to be accurate when $r^* < R^*$ and yet sufficiently large such that the approximation $c(r^*) = a(h(r^*), u(r^*))$ is accurate when $r^* > R^*$. Thus, a simple approach is to choose R^* as the location of the third zero of h, as this is always found in the plateau region. The approach may not be reliable when $\rho^* \leq 0.4$, as no plateau is seen under those conditions and is not possible at the low densities where h does not have a third zero. However, principal objectives of thermodynamic property prediction by molecular simulations are moderate to high densities where this location for R^* will exist. The results presented below have been obtained using the third zero for R^*.

4.2 LJ fluid

Figure 4 compares the isothermal compressibilities obtained from the KB integral approach (Equation (11)) using each of the three expressions for c (Equations (12)–(14)) with those from the EOS. Qualitatively, the three approaches are consistent with each other, as well as with the EOS at all four temperatures. Furthermore, the results obtained using the Mayer f-function are very similar to those obtained using the PY relation. The results obtained using these two approaches are typically within 1–5% of the EOS. The situation is not as good at the two lowest temperatures; the differences are as high as 7 and 9% for the Mayer function and the PY relation, respectively. The greatest disagreement is seen when $T^* = 1.5$ and ρ^* is 0.2, 0.3 or 0.4, which are state points closest to the critical point $\rho_c^* = 0.304$, $T_c^* = 1.316$ [30]. At those conditions, the differences are 9–20%. This disagreement is not

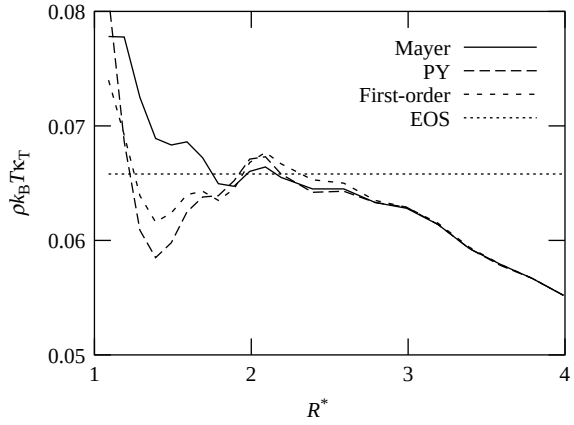

Figure 3. Isothermal compressibilities obtained from KB integrals as a function of R^* at $T^* = 1.5$, $\rho^* = 0.8$.

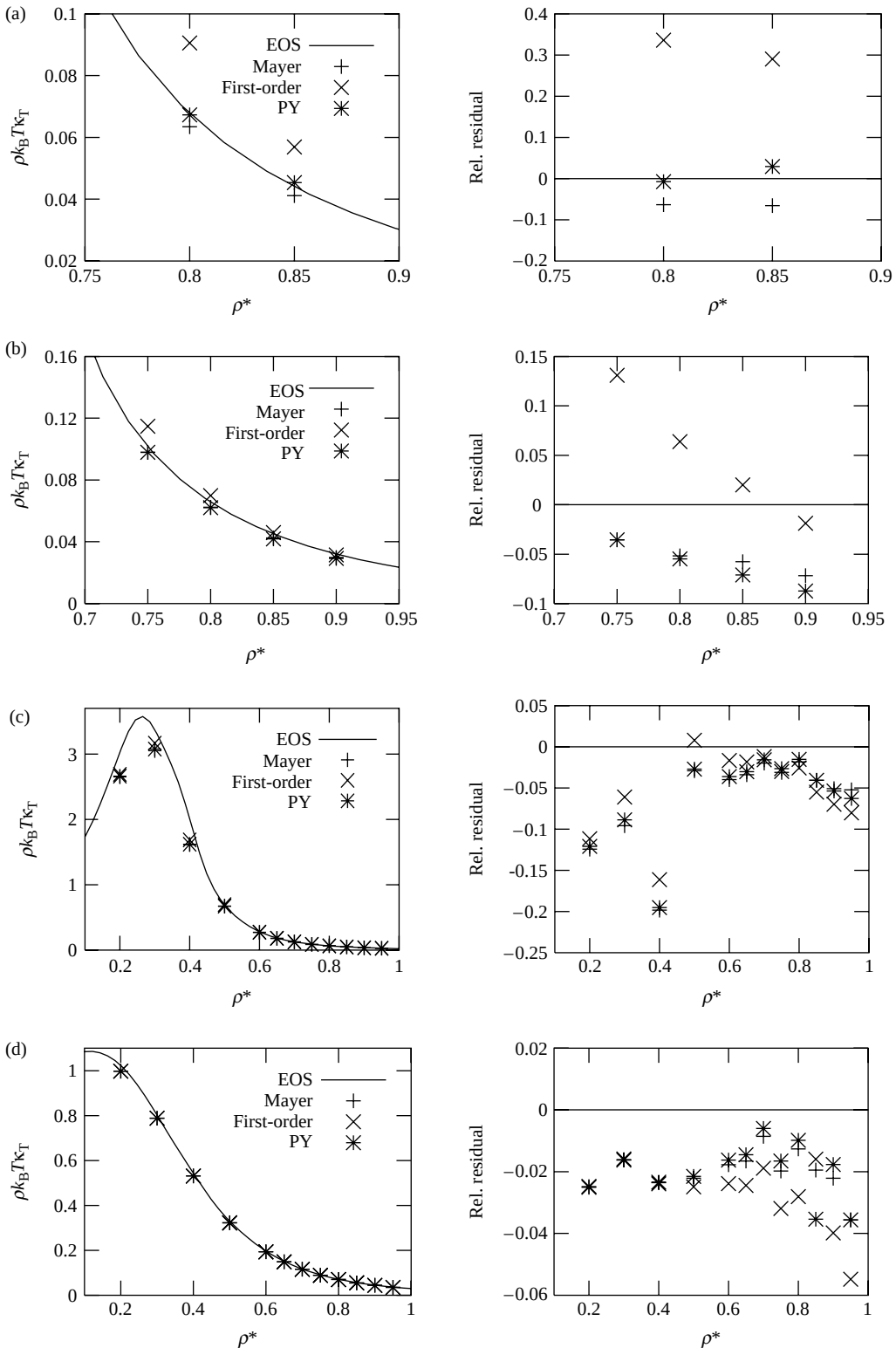

Figure 4. Results and relative residuals from calculations with R^* taken as the third zero of h, at temperatures (a) $T^* = 0.85$, (b) $T^* = 1.0$, (c) $T^* = 1.5$ and (d) $T^* = 2.5$. Values derived from the EOS by Mecke et al. [28] are also shown.

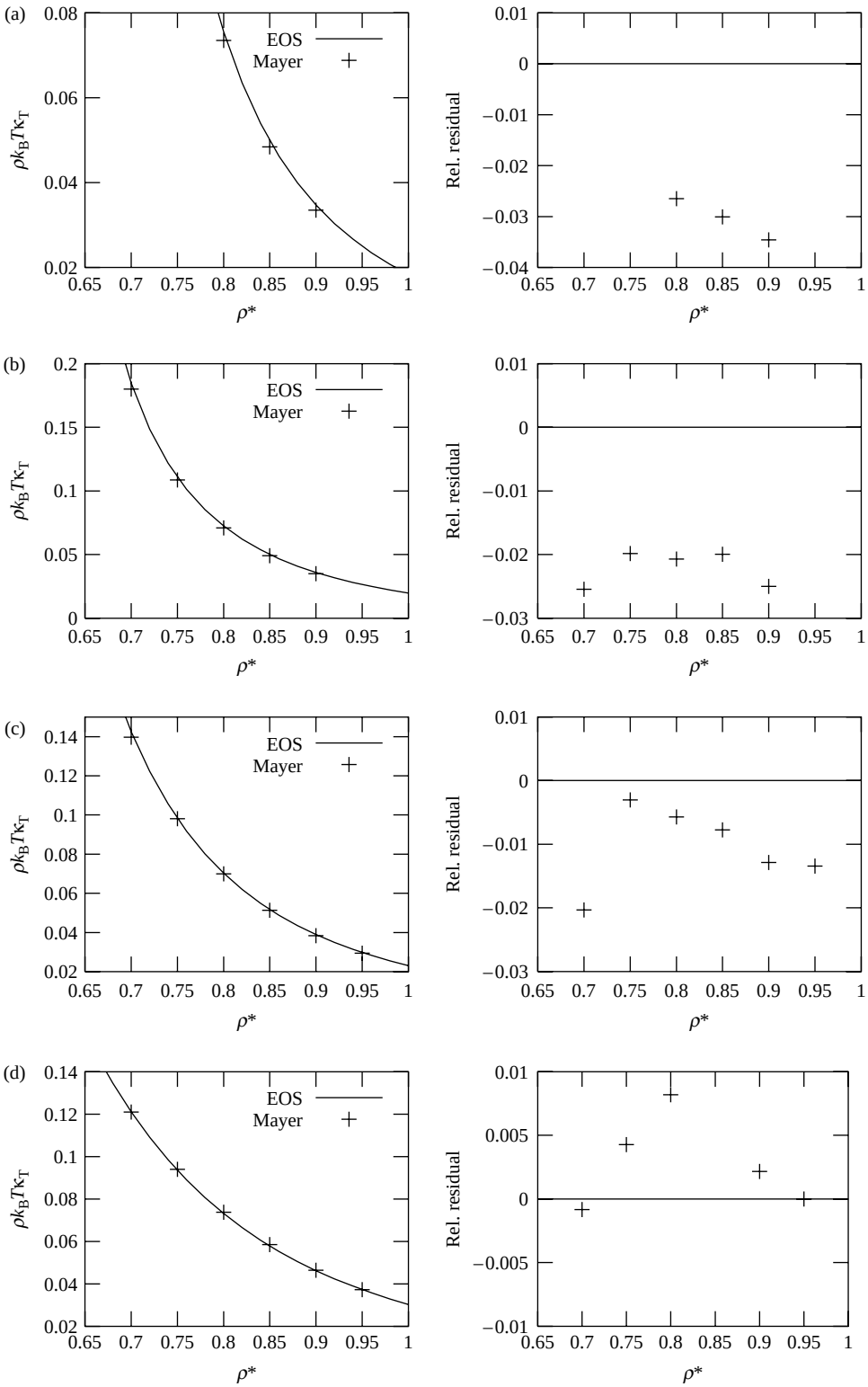

Figure 5. Results and relative residuals for the Stockmayer fluid with $\mu^{*2} = 1$, at temperatures (a) $T^* = 1.0$, (b) $T^* = 1.15$, (c) $T^* = 1.5$ and (d) $T^* = 2.5$. Values derived from the EOS by Gross and Vrabec [29] are also shown.

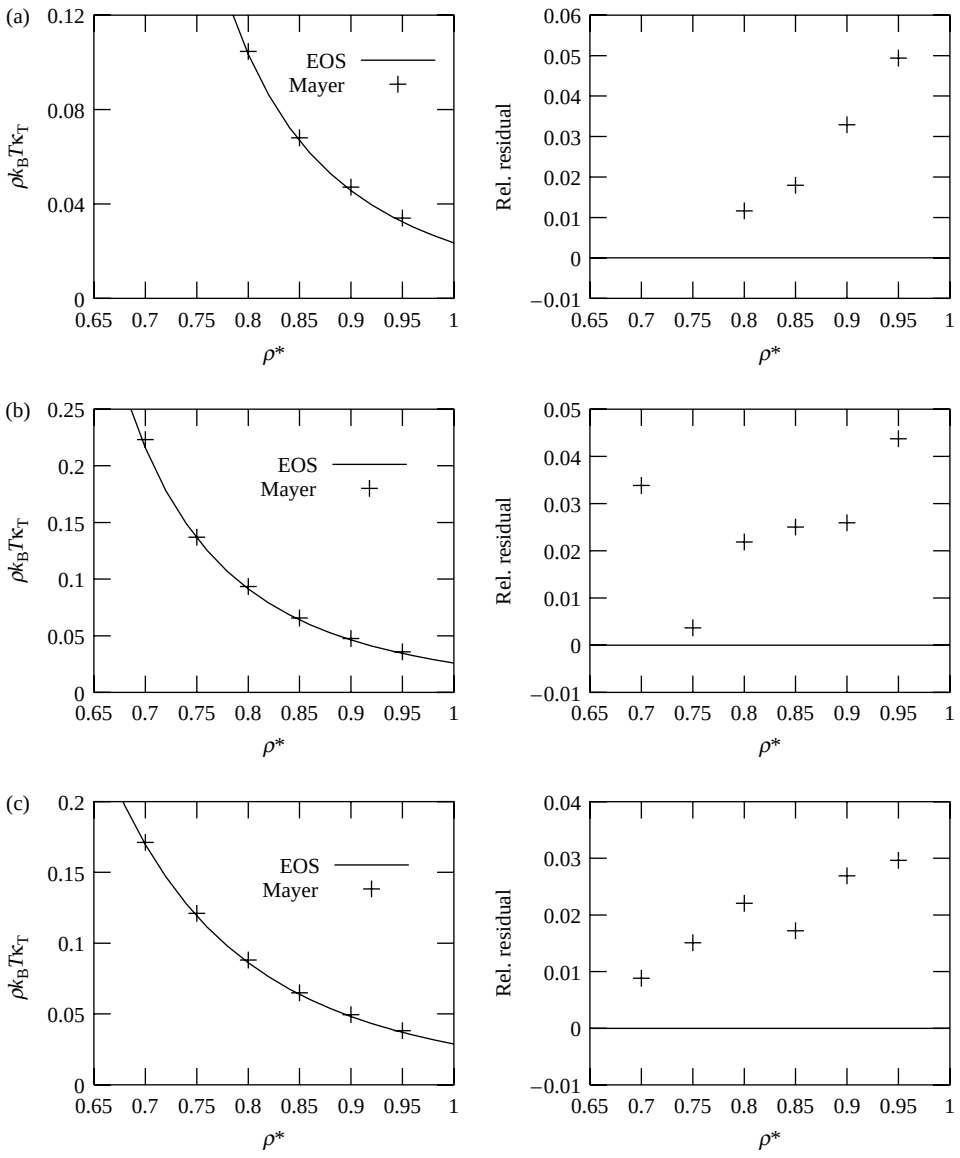

Figure 6. Results and relative residuals for the Stockmayer fluid with $\mu^{*2} = 3$, at temperatures (a) $T^* = 1.3$, (b) $T^* = 1.6$ and (c) $T^* = 2.0$. Values derived from the EOS by Gross and Vrabec [29] are also shown.

surprising considering that the quantity $1 - C$ can be very small in this region and the integrand of the DCFI has nearly equal positive and negative portions. Thus, the compressibility as given by Equation (6) will be more sensitive to the asymptotic expression for $c(r)$ when $r > R$. For $\rho^* = 0.7$ and 0.8, the agreement with the EOS is better at higher temperature (1% at $T^* = 2.5$) than at lower temperature (6% at $T^* = 0.85$).

The results obtained using the first-order density expansion for c appear to be consistent with the two other approaches at the supercritical temperatures, but the results diverge and differ by 5–40% at the subcritical temperatures. At these temperatures, the results are also in far worse agreement with the EOS. The large differences in results from Equation (13) compared to those from Equations (12) and (14) are due to that the convolution term in Equation (13) is larger at low temperatures. At $T^* = 0.85$ and 1.0, the term becomes greater than unity at $r \approx R \approx 2$. Consequently, the tail given by the first-order density expansion differs significantly from that given by the Mayer *f*-function.

The temperature effects on the accuracy of the KB integrals can be understood by considering Equation (10) where we see that the tail contribution of the DCF increases in magnitude with decreasing temperature. It is thus likely that the presumably small error introduced by forcing the tail to follow Equations (12)–(14) results in errors in κ_T that are more pronounced at low temperatures. It is also possible that derivatives of the Mecke EOS [28] could be less accurate at lower temperature since differences

in pressure with simulations are greater than at higher temperature. Nevertheless, though low temperatures seem to offer more of a challenge, we still consider the results obtained under those conditions to be satisfactory.

Statistical errors in the results were estimated for a few representative state points using the blocking method [24], considering blocks of 100 ps to be independent. The standard error in κ_T was found to be $<0.5\%$ of κ_T itself. This indicates that the calculation of this property is well converged for simulations of the current length.

4.3 *Stockmayer fluid*

The results obtained from the Stockmayer simulations with $\mu^{*2} = 1$ are shown in Figure 5. Given the discussion above, we now focus on the high-density region $0.70 \leq \rho^* \leq 0.95$, where the lower bound approximately corresponds to $2\rho_c^*$, with $\rho_c^* = 0.317$ being the density at the critical point as given by the Gross EOS [29]. Under those conditions, the isothermal compressibilities obtained from the KB integral are within 3–4% of those obtained from the Gross EOS [29], for all temperatures. This is good agreement, considering that the pressures typically disagree by 0.5–2.5%. We note that, consistent with the LJ results, the agreement improves with increasing temperature. The error is, for example, around 3% when $T^* = 1.0$, while it is $<1\%$ when $T^* = 2.5$. We do not observe any tendency for the agreement to depend on density, as long as $\rho^* > 1.5\rho_c^*$. When $T^* = 1.5$, just above the critical temperture, $T_c^* = 1.45$ [29] the results compare well with the Gross EOS [29] when the density is high, but accuracy deteriorates at lower densities in the near-critical region (not shown in Figure 5). Under conditions where ρ^* is 0.3 or 0.4, the simulation results for κ_T deviate from the Gross EOS [29] values by up to 40%. This is similar to the behaviour for the LJ fluid at $T^* = 1.5$.

The results from the simulations using $\mu^{*2} = 3$ are shown in Figure 6. The compressibilities obtained from simulation agree with the ones obtained from the Gross EOS [29] to within 5%. This is slightly worse than for $\mu^{*2} = 1$, but still acceptable considering that the agreement of pressures is also worse for the higher dipole moment. Just as for the lower dipole moment and for the LJ fluid, the agreement improves as the temperature gets higher and the density is lower.

Although the Stockmayer potential is anisotropic, we obtain good results in the high-density region suggesting that the computational methodology based on Equation (4), which neglects the coupling between the isotropic and anisotropic parts of the correlation functions, is accurate.

5. Conclusions

We have evaluated the accuracy of isothermal compressibilities obtained by integrating the total and direct correlation functions obtained from molecular simulations of the pure LJ and Stockmayer fluids, as extended by Verlet's method [13]. We have employed several theories for describing the behaviour of $c(r)$ at large r and found that the Mayer f-function yields good results and is the most appropriate one to use when we seek to extend the method to more realistic fluid models. At densities above $1.5 - 2\rho_c$, the results are in good agreement with the Mecke and Gross EOS [28,29]. For both fluids, the agreement is best at high temperatures while it is less for state points in the near-critical region.

Our study of the anisotropic Stockmayer fluid has shown that good results can be obtained with the approximate 'atomic' OZ equation, Equation (4). It is possible that the results for non-spherical repulsive forces would be less accurate, since such forces have a greater effect on the radial distribution function than multipolar forces [19,31]. Nevertheless, the results of Gubbins and O'Connell [32] suggest that κ_T is rather insensitive to the anisotropic forces as long as $\rho > 2\rho_c$, even for molecular liquids.

The results presented here show that accurate results can be obtained for pure fluids. This encourages further work on extending the methodology to mixtures, as this could enable calculation of very useful quantities, such as activities.

Acknowledgements

The authors gratefully acknowledge access to the Danish Center of Scientific Computing at the University of Southern Denmark, Odense, Denmark. R.W. acknowledges financial support from IP Bioproduction, within the Sixth Framework Programme of the European Union. G.H.P. acknowledges financial support from the Danish National Research Foundation via a grant to MEMPHYS.

References

[1] J.J. de Pablo and F.A. Escobedo, *Molecular simulations in chemical engineering: Present and future*, AIChE J. 48 (2002), pp. 2716–2721.
[2] W.F. van Gunsteren, *Computer Simulation of Biomolecular Systems: Theoretical and Experimental Applications*, ESCOM Science Publishers, Leiden, 1989.
[3] S. Christensen, G.H. Peters, F.Y. Hansen, J.P. O'Connell, and J. Abildskov, *State conditions transferability of vapor–liquid equilibria via fluctuation solution theory with correlation function integrals from molecular dynamics simulation*, Fluid Phase Equilibr. 260 (2007), pp. 169–176.
[4] S. Christensen, G.H. Peters, F.Y. Hansen, and J. Abildskov, *Thermodynamic models from fluctuation solution theory analysis of molecular simulations*, Fluid Phase Equilibr. 261 (2007), pp. 185–190.
[5] S. Christensen, G.H. Peters, F.Y. Hansen, J.P. O'Connell, and J. Abildskov, *Generation of thermodynamics data for organic liquid mixtures from molecular simulations*, Mol. Simul. 33 (2007), pp. 449–457.
[6] J.G. Kirkwood and F.P. Buff, *The statistical mechanical theory of solutions. I*, J. Chem. Phys. 19 (1951), pp. 774–777.
[7] J.P. O'Connell, *Thermodynamic properties of solutions based on correlation functions*, Mol. Phys. 20 (1971), pp. 27–33.

[8] J.J. Salacuse, A.R. Denton, and P.A. Egelstaff, *Finite-size effects in molecular dynamics simulations: Static structure factor and compressibility. I. Theoretical method*, Phys. Rev. E 53 (1996), pp. 2382–2389.
[9] S. Weerasinghe and P.E. Smith, *Kirkwood–Buff derived force field for mixtures of acetone and water*, J. Chem. Phys. 118 (2003), pp. 10663–10670.
[10] A. Perera and F. Sokolić, *Modeling nonionic solutions: The acetone–water mixture*, J. Chem. Phys. 121 (2004), pp. 11272–11282.
[11] B. Hess and N.F.A. van der Vegt, *Cation specific binding with protein surface charges*, Proc. Natl Acad. Sci. 106 (2009), pp. 13296–13300.
[12] R. Wedberg, G.H. Peters, and J. Abildskov, *Total correlation function integrals and isothermal compressibilities from molecular simulations*, Fluid Phase Equilibr. 273 (2008), pp. 1–10.
[13] L. Verlet, *Computer 'experiments' on classical fluids. II. Equilibrium correlation functions*, Phys. Rev. 165 (1968), pp. 201–214.
[14] D.L. Jolly, B.C. Freasier, and R.J. Bearman, *The extension of simulation radial distribution functions to an arbitrary range by Baxter's factorisation technique*, Chem. Phys. 15 (1976), pp. 237–242.
[15] M. Dixon and P. Hutchinson, *A method for extrapolation of pair distribution functions*, Mol. Phys. 33 (1976), pp. 1663–1670.
[16] S.J. Galam and J.P. Hansen, *Statistical mechanics of dense ionized matter: Electron screening corrections to the thermodynamic properties of the one-component plasma*, Phys. Rev. A 14 (1976), pp. 816–832.
[17] D.M. Ceperley and G.V. Chester, *Perturbation approach to the classical one-component plasma*, Phys. Rev. A 15 (1977), pp. 755–764.
[18] S.M. Foiles, N.W. Ashcroft, and L. Reatto, *Structure factor and direct correlation function of a fluid from finite range simulation data*, J. Chem. Phys. 81 (1984), pp. 6140–6145.
[19] G. Gray and K.E. Gubbins, *Theory of Molecular Fluids, Volume 1: Fundamentals*, Oxford University Press, New York, NY, 1984.
[20] S.W. Brelvi and J.P. O'Connell, *A corresponding states correlation of liquid compressibilities and partial molar volumes of gases at infinite dilution*, AIChE J. 18 (1972), pp. 1239–1243.
[21] Y.H. Huang and J.P. O'Connell, *Corresponding states correlation for the volumetric properties of compressed liquids and liquid mixtures*, Fluid Phase Equilib. 37 (1987), pp. 75–84.
[22] D.A. McQuarrie, *Statistical Mechanics*, Harper & Row, New York, NY, 1976.
[23] T.M. Reed and K.E. Gubbins, *Applied Statistical Mechanics*, McGraw-Hill, New York, NY, 1973.
[24] M.P. Allen and D.J. Tildesley, *Computer Simulation of Liquids*, Oxford University Press, New York, NY, 1987.
[25] D.C. Rapaport, *The Art of Molecular Dynamics Simulation*, Cambridge University Press, Cambridge, 2004.
[26] J.L. Lebowitz and J.K. Percus, *Asymptotic behavior of the radial distribution functions*, J. Math. Phys. 4 (1974), pp. 248–254.
[27] W.H. Press, *Numerical Recipes in C: The Art of Scientific Computing*, Cambridge University Press, Cambridge, 1992.
[28] M. Mecke, A. Müller, J. Winkelmann, J. Vrabec, J. Fischer, R. Span, and W. Wagner, *An accurate van der Waals-type equation of state for the Lennard-Jones fluid*, Int. J. Thermophys. 17 (1996), pp. 391–404.
[29] J. Gross and J. Vrabec, *An equation of state contribution for polar components: Dipolar molecules*, AIChE J. 52 (2006), pp. 1194–1204.
[30] B. Smit, *Phase diagrams of Lennard-Jones fluids*, J. Chem. Phys. 96 (1992), pp. 8639–8640.
[31] S.S. Wang, C.G. Gray, P.A. Egelstaff, and K.E. Gubbins, *Monte Carlo study of the pair correlation function for a liquid with non-central forces*, Chem. Phys. Lett. 21 (1973), pp. 123–126.
[32] K.E. Gubbins and J.P. O'Connell, *Isothermal compressibility and partial molal volume for polyatomic liquids*, J. Chem. Phys. 60 (1974), pp. 3449–3453.